JCTC Journal of Chemical Theory and Computation

Article

pubs.acs.org/JCTC

QM/MM Study of Substituent and Solvent Effects on the Excited State Dynamics of the Photoactive Yellow Protein Chromophore

Francisco F. García-Prieto,[†] Aurora Muñoz-Losa,[†] Ignacio Fdez. Galván,[2] M. Luz Sánchez,[†] Manuel A. Aguilar,[†] and M. Elena Martín*[,†]

[†]Área de Química Física, University of Extremadura, Avda. Elvas s/n, Edif. José Mª Viguera Lobo 3ª planta, Badajoz, 06006 Spain

[2]Department of Chemistry—Ångström, The Theoretical Chemistry Programme, Uppsala University, Box 518, 751 20 Uppsala, Sweden

Supporting Information

ABSTRACT: Substituent and solvent effects on the excited state dynamics of the Photoactive Yellow Protein chromophore are studied using the average solvent electrostatic potential from molecular dynamics (ASEP/MD) method. Four molecular models were considered: the ester and thioester derivatives of the *p*-coumaric acid anion and their methylated derivatives. We found that the solvent produces dramatic modifications on the free energy profile of the S1 state: 1) Two twisted structures that are minima in the gas phase could not be located in aqueous solution. 2) Conical intersections (CIs) associated with the rotation of the single bond adjacent to the phenyl group are found for the four derivatives in water solution but only for thio derivatives in the gas phase. 3) The relative stability of minima and CIs is reverted with respect to the gas phase values, affecting the prevalent de-excitation paths. As a consequence of these changes, three competitive de-excitation channels are open in aqueous solution: the fluorescence emission from a planar minimum on S1, the *trans*—*cis* photoisomerization through a CI that involves the rotation of the vinyl double bond, and the nonradiative, nonreactive, de-excitation through the CI associated with the rotation of the single bond adjacent to the phenyl group. In the gas phase, the minima are the structures with the lower energy, while in solution these are the conical intersections. In solution, the de-excitation prevalent path seems to be the photoisomerization for oxo compounds, while thio compounds return to the initial *trans* ground state without emission.

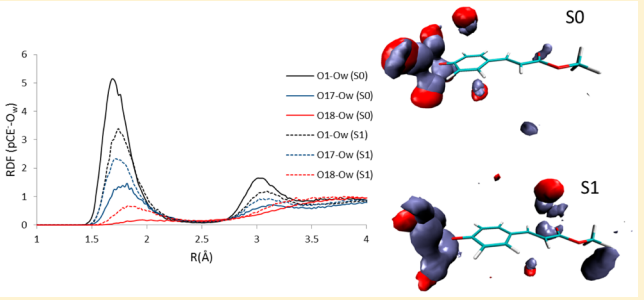

I. INTRODUCTION

The Photoactive Yellow Protein (PYP)[1−7] is responsible for the negative phototaxis of *Halorhodospira halophila*[1,2] in the presence of blue light.[8] The PYP is a small cytoplasmic protein with 125 amino acids and a single chromophore, the anionic form of the *p*-coumaric acid (pCA^-), which binds to the protein through a covalent thioester bond with the amino acid cysteine[3,4] (Cys-69), see Figure 1.

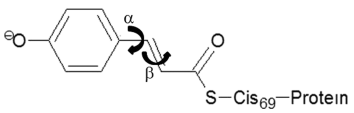

Figure 1. PYP chromophore.

Several studies have addressed the structural changes in PYP that trigger the biological response in the bacterium.[9−12] After the absorption of radiation the *trans*—*cis* photoisomerization (in a time scale of the order of subpicosecond) of the vinyl double bond[13−15] (marked as β in Figure 1) takes place. It is commonly accepted that the *trans*—*cis* photoisomerization of the chromophore occurs through a conical intersection between the first excited state S1 and the ground state S0,[16−20] a process that mirrors the retinal transformation in rhodopsin during the vision process.[21,22] Along with rhodopsin, the PYP is one of the most studied photosensitive biological systems from both an experimental and theoretical point of view.

In the gas phase, the excited states of the anionic derivatives of *p*-coumaric acid are not stable and undergo autoionization,[23−26] which makes difficult a direct comparison of the de-excitation channels in the gas phase and inside the protein. In order to highlight the effect of the protein on the photoisomerization of the chromophore, it is convenient to address it in solution studies. Experiments[11,27] have shown that in polar solvents the excited state of the PYP chromophore, the thioester derivative of deprotonated *trans*-*p*-coumaric acid, $pCTE^-$, de-excites without formation of the *cis* conformer. On the contrary, the UV—visible absorption spectrum of the ester derivative, pCE^-, in basic solution of methanol under steady-state irradiation displays an isosbestic point that has been attributed to the partial formation of the *cis* isomer.[28] Larger

Received: November 2, 2016
Published: January 10, 2017

DOI: 10.1021/acs.jctc.6b01069
J. Chem. Theory Comput. 2017, 13, 737−748

photoisomerization yields have been found in the amide and dianionic derivatives. In order to explain these facts, it has been proposed[12,17] that in polar solvents there are three competitive de-excitation channels: 1) the fluorescence emission, 2) the *trans*−*cis* photoisomerization involving the rotation around the vinyl double bond, and 3) a nonradiative, nonreactive, de-excitation that involves the rotation around the single bond adjacent to the phenyl group (marked as α in Figure 1). Additionally, Gromov et al.[20] have recently proposed that the out-of-plane motion of the hydrogen atoms of the ethylenic bond is coupled to the two torsional modes.

An important point that seems to determine the evolution of the excited state is that the α-torsion has a lower energy barrier than the β torsion. Groenhof et al.[16,29,30] proposed that both torsions occur in the protein, although the turn in α does so to a much lower extent. In the protein, the photoisomerization seems to be favored by chromophore−protein interactions, while steric hindrance prevents the torsion in α.[30−35] Gromov et al.[36,37] suggest a link between the two torsions so that the twist in β cannot occur without a slight twist in α. Although the torsion in α has not yet been experimentally confirmed, a recent study reported that *trans*−*cis* isomerization is inhibited if the torsion in α is completely suppressed.[38]

In order to identify and understand the factors governing the S1 excited state fate it is compulsory to have a good description of the topology of its potential energy surface. This task is complex as the critical point structures (minima, transition states, conical intersections) vary with the calculation level[19,37] and the nature of the surrounding medium. Various studies[15,20,39,40] have shown that the photoisomerization is accompanied by changes in the hydrogen bond network that the chromophore establishes with the surrounding environment. These interactions can be analyzed by comparing the chromophore experimental absorption spectra in the protein[3] with those recorded in the gas phase[24,41] and in solution.[28,42] Experimental[31] and theoretical[43,44] studies have confirmed that hydrogen bonds stabilize the negative charge hosted by the phenolic end[45,46] and prevent the chromophore autoionization that occurs in the gas phase. Unfortunately, there is still controversy about the actual role played by solvent[12,47−50] or by some PYP amino acids such as Arg-52[16,17,19,29,30,38] and Cys-69.[51,52]

Several molecules have been proposed as models for the study of the PYP chromophore. Although results between different molecular models are comparable in the gas phase,[53,54] the consideration of intermolecular interactions introduces additional difficulties because not all models interact in the same way with the environment. Espagne et al.,[27] for instance, studied several models: the fully deprotonated form of the *p*-coumaric acid (pCA^{2-}), the amine derivative in the carbonyl end (pCM^{-}), and the thiophenyl ester derivative (pCT^{-}) among others. Absorption and emission spectra showed that for pCM^{-} and pCA^{2-} the main de-excitation channel was a *trans*−*cis* isomerization. Instead, pCT^{-} follows an alternative nonreactive channel in which an intermediate was detected with an absorption band at 450 nm (2.76 eV). Other experiments have also detected this intermediate in basic solutions of the thiomethyl ester derivative ($pCTE^{-}$[23,5556]).

In the present study we describe the main critical points on the S1 excited state in four PYP chromophore models (methyl ester, pCE^{-}; thiomethyl ester, $pCTE^{-}$; acid, pCA^{-}; and thioacid, $pCTA^{-}$) both in the gas phase and water (Figure 2). The ultimate goal is to use this information to determine

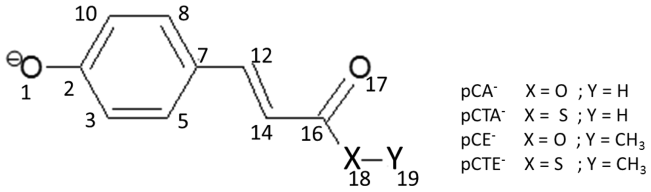

Figure 2. PYP chromophore derivatives studied in the present study: acid (pCA^{-}), thioacid ($pCTA^{-}$), methyl ester (pCE^{-}), and methyl thioester ($pCTE^{-}$).

the key factors that favor one or another deactivation channel in aqueous solution. The rest of the paper is organized as follows: Section II describes the methods used in the study. Section III provides some technical details. Section IV analyzes the main results. First, the topology of the first excited state for the four derivatives is described in the gas phase. Then, solvent effects on emission spectra and nonradiative de-excitation channels are analyzed, comparing our results with the available experimental and theoretical data. Finally, in Section V the main conclusions are presented.

II. METHOD

Solvent effects on the geometry and electronic structure of several derivatives of the *p*-coumaric acid were calculated using the averaged solvent electrostatic potential from molecular dynamics data (ASEP/MD) method[57−62] developed in our laboratory. This is a sequential quantum mechanics/molecular mechanics (QM/MM) method implementing the mean field approximation. In this approximation, the average value of any solute property is replaced by the value calculated in the presence of an average perturbation. Details of the method have been described in previous papers,[57−62] so here we will only present a brief outline.

As mentioned above, ASEP/MD is a method combining QM and MM techniques, with the particularity that full QM and MD (Molecular Dynamics) calculations are alternated and not simultaneous. From the MD simulation, the average electrostatic potential generated by the solvent on the solute (ASEP) is obtained. This potential is introduced as a perturbation into the solute's quantum mechanical Hamiltonian, and by solving the associated Schrödinger equation, one gets a new charge distribution for the solute and a new geometry if an optimization is performed, which are used in the next MD simulation. This iterative process is repeated until the electron distribution of the solute, its geometry, and the solvent structure around it become mutually equilibrated.

The in solution geometries are obtained using a technique described in a previous paper[62] and based on the joint use of the free-energy gradient method[63−65](FEG) and the mean field approximation.[66] The technique has been successfully applied to the geometry optimization of ground and excited states of molecules in solution. It is worthy of note that in the FEG method a rigid body approximation is used for the solute, i.e., the solute geometry is kept fixed during the MD calculation. Next, the solvent contribution to the mean values of the total force, *F*, and Hessian, *G*, is calculated from a representative set of solvent configurations and subsequently added to the internal solute contribution during the quantum calculation.

Minimum energy conical intersections (MECIs) were located using a modification of the Martínez's algorithm[67] implemented in the ASEP/MD method. The main advantage of Martínez's method is that it is not necessary to calculate

DOI: 10.1021/acs.jctc.6b01069
J. Chem. Theory Comput. 2017, 13, 737−748

derivative couplings; only difference gradients are required. The method is based in seeking a minimum of the objective function F_{IJ}. This function is the sum of two terms: the first one corresponds to the average of the energies of the two states involved in the CI, and the second one is a penalty function that monotonically increases with the energy gap

$$\frac{dF_{IJ}(\vec{R};\sigma;\alpha)}{d\vec{R}} = \frac{1}{2}\left(\frac{dE_I(\vec{R})}{d\vec{R}} + \frac{dE_J(\vec{R})}{d\vec{R}}\right) + \sigma\frac{\Delta E_{IJ}^2 + 2\alpha\Delta E_{IJ}}{(\Delta E_{IJ} + \alpha)^2}\left(\frac{dE_I(\vec{R})}{d\vec{R}} - \frac{dE_J(\vec{R})}{d\vec{R}}\right) \quad (1)$$

where E_I and E_J are the energies of the two crossing states, α is a smoothing parameter, and σ is a parameter that increases until $\Delta E \leq \delta$, δ being a cutoff whose value is fixed before starting the calculations. In this point, it is worth mentioning some considerations about the implementation of the Martínez's algorithm in ASEP/MD. First, when the system is in solution, energies and gradients used in the MECI search are replaced by free energies and derivatives of the free energy, respectively. Second, when the system is approaching the CI and in order to avoid instabilities, the solvent is equilibrated always with the same electronic state independently of the CASSCF root order (the state is selected based on the dipole moment value). Finally, solvent dynamic effects are neglected, i.e., it is assumed that the solvent is always in equilibrium with the charge distribution of the excited state, that is, the CI is optimized in a subset of all the possible solvent configurations (equilibrium + nonequilibrium configurations), from this point of view the MECI energy thus obtained is an upper limit to the actual value. However, as we show below, in the PYP chromophore the two CIs involved in the nonradiative deactivations are the lowest energy points on S1; in fact, they can be located by minimizing directly the free energy of the S1 state. Consequently, in the studied systems the optimization procedure permits to obtain the real MECIs. ASEP/MD has previously been successfully applied to the study of de-excitation paths in acrolein[68,69] and retinal.[70]

Once the solute electronic states and the solvent structure around them have been optimized and equilibrated, free energy differences between states can be calculated making use of a dual method, where the solute contributions are quantum-mechanically calculated, but solvent contributions are evaluated classically. The expression we use to calculate the free energy difference between two species or states, I and J, in solution, ΔG_{IJ}, is

$$\Delta G_{IJ} = \Delta E_{IJ} + \Delta G_{IJ}^{\text{int}} + \Delta V_{IJ} \quad (2)$$

where ΔE is the difference in the internal quantum energy of the solute between the two species or states I and J, ΔG^{int} is the solute–solvent interaction free energy difference, which is calculated classically with the free energy perturbation (FEP)[71] method, and ΔV is a term that includes the zero point energy difference and entropic contributions between the two states. This last term is evaluated by applying the harmonic oscillator and rigid rotor approximations to the vibrational and rotational modes of the solute in solution, and it needs the information provided by the Hessian matrix, something that makes its calculation difficult for in solution systems. In a previous study[72] it was found that the contribution of this term to the excited state conformational equilibrium of pCE^- in the gas phase was 0.07 eV. Because of its low value and its large computational cost in solution, this component has been neglected, and its value is not included in final results.

III. COMPUTATIONAL DETAILS

Solvent effects on the radiative and nonradiative deactivation channels of four molecular models of the deprotonated PYP chromophore were studied with the ASEP/MD method,[57−62] using Molcas-7.4[73] and Gromacs-4.5[74,75] programs for quantum calculations and molecular dynamics simulations, respectively. The iterative ASEP/MD procedure stops when convergence in the QM energy (0.0001 au) is reached. This is achieved in about 10−15 cycles.

Geometry optimization was performed with the complete active self-consistent field (CASSCF) theory both in the gas phase and in solution. Based on our previous experience in studying the *p*-coumaric acid system, the selected basis set was cc-pVDZ.[76] The active space was formed by 12 electrons in 11 orbitals, all of π nature. Excited state structures (Franck–Condon points, minima, and conical intersections) were calculated as the state averaged of the first two states (SA2), considering equal weights. Whereas CASSCF takes into account the near-degeneracies of different electronic configurations, the dynamic correlation energy is not included. This component was considered by using CASPT2 methodology.[77,78] In these calculations, the SA2-CASSCF wave functions were used as reference. A value of 0.0 for the ionization potential–electron affinity (IPEA) shift in CASPT2 calculations was used. This IPEA value was chosen for both theoretical concerns (for a very interesting discussion about the convenience or not of IPEA corrections see Zobel et al.[79]) and numerical suitability (the commonly recommended 0.25 IPEA value was estimated in the complete basis set limits, for the basis set of small or medium size—as is cc-pDVZ—the use of this value moves away the calculated transition energies from the experimental values). To minimize the appearance of intruder states, an imaginary shift of 0.1i E_h was considered. Oscillator strengths were calculated with the RASSI algorithm implemented in Molcas-7.4.[73]

In solution transition energies were calculated assuming frozen solvent conditions. Consequently, the ASEP/MD iterative process was only performed on the initial state of the transition (the ground state for absorption, the excited state for emission); i.e., the atomic charges used during the MD and the energy derivatives employed in the geometry optimization of the solute are calculated with the initial state's wave function. Then, the energies of the final states are obtained.

Molecular dynamics simulations included 1532 water molecules and one molecule of solute in a rhombic dodecahedral box. No counterion was included. Previous studies[80] in a related system have shown that, because of the large dielectric screening effect of polar solvents, the effect of the counterion on the structure and spectrum of the chromophore is minimal. For the solute, the Lennard-Jones parameters were taken from the optimized potentials for liquid simulations, all atoms (OPLS-AA) force field.[81,82] The atomic charges of the solute molecules were obtained using the CHELPG (Charges from Electrostatic Potential, Grid) method. The charges were updated at each ASEP/MD cycle. The solvent was described using a nonpolarizable force field. It is known that the solvent polarization could represent an important contribution to the total solvent shift;[83,88] however, in the case of monoanionic derivatives of the *p*-coumaric acid it has been shown[88] that this contribution is negligible, and it will

DOI: 10.1021/acs.jctc.6b01069
J. Chem. Theory Comput. 2017, 13, 737−748

not be considered in our study. For water molecules, the TIP4P[84] model was employed. Periodic boundary conditions were applied in all directions. Short-range electrostatic interactions were cut off at 1.3 nm, and long-range interactions were calculated with the Particle-Mesh Ewald (PME) method.[85] The temperature was fixed at 298 K with the Nosé−Hoover thermostat.[86,87] Each simulation was run in the NVT ensemble for 500 ps, with a time step of 1 fs, where the first 200 ps were used for equilibration and the last 300 ps for production. In solution final results were obtained by averaging the last five ASEP/MD cycles, and therefore they represent a 1.5 ns average.

The solute−solvent interaction contribution, ΔG_{IJ}^{int}, to the total free energy differences was calculated with the free energy perturbation (FEP) method.[88] The solute geometry was assumed to be rigid and a function of the perturbation parameter λ. When $\lambda = 0$, the solute geometry and charges correspond to the initial state (the chromophore ground state, for instance). When $\lambda = 1$, the charges and geometry correspond to the final state (the critical points on the chromophore excited state surface). Charges and geometries of the initial and final states are those obtained with ASEP/MD. A linear interpolation is applied for intermediate values. A value of $\Delta\lambda = 0.005$ was used. That means that a total of 200 separate molecular dynamics simulations were carried out to determine each free-energy difference. The final value is obtained as the arithmetic mean of the backward and forward free energy values.

IV. RESULTS AND DISCUSSION

a. Excited State Potential Energy Surfaces in the Gas Phase. It is worth reminding that the excited states of the anionic derivatives of the *p*-coumaric acid can undergo autoionization[23−26] in the gas phase and that they become stable only in polar solvents or in any other medium where their negative charge could be stabilized. Despite this, the study of gas phase excited states is interesting as it can help to clarify the protein or solvent effects on the free energy surfaces of the excited states and, consequently, on the de-excitation processes.

CASSCF geometry optimizations of the first excited state, S1, lead to three minima: a planar structure (denoted as $S1^p$) and two twisted minima (denoted as $S1^\alpha$ and $S1^\beta$), corresponding to the rotation of the single bond adjacent to the phenyl group and the rotation of the vinyl double bond, respectively. Geometric parameters for the ground and $S1^p$ excited state minima of the four anionic molecular models can be found in Table S1 of the Supporting Information. The $S1^p$ minima have dihedral and bond angles similar to the ground state minima, S0, and hence to the FC point. The S0 geometry is the result of the equilibrium between two resonance forms (see Figure 3), with the negative charge localized at the phenolate oxygen or at the carboxyl fragment. The four molecular models display a quinolic character, the C3−C5 and C8−C10 bond lengths being shorter than the rest of the ring C−C bond lengths. The quinolic character is lower in the $S1^p$ excited state than in the ground state. The main differences between the $S1^p$ excited state geometries of the four molecular models arise in the C7−C12 and C12−C14 bond lengths. Thus, the C7−C12 bond (the single bond adjacent to the ring) is shorter in the pCE^-/pCA^- pair (about 0.01 Å) than in the $pCTE^-$/$pCTA^-$ pair. The opposite is found in the C12−C14 bond (central double bond), being larger in the pCE^-/pCA^- pair than in $pCTE^-$/$pCTA^-$ (1.413 Å vs 1.408 Å). As a result of these differences, rotations around the double bond are expected to be easier for oxo compounds than for thio compounds, while α-rotations should be easier for thio compounds.

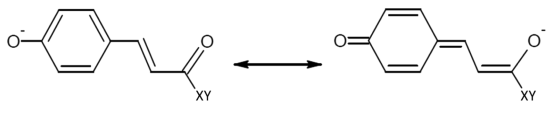

Figure 3. Resonance forms for the PYP chromophore.

Table S2 of the Supporting Information summarizes some geometric parameters for twisted minima. The $S1^\alpha$ structures show an α-twist of around 90° without rotation around β. In the same way, the $S1^\beta$ stationary points are characterized by a torsional angle of $\beta \approx 90°$ and almost no twist around α (see Figure 4). When these geometries are compared with the $S1^p$ structure (Table S1), it can be verified that the quinolic character is stronger in $S1^\alpha$ and $S1^\beta$ than in $S1^p$, as the C2−C3, C5−C7, C7−C8, and C2−C10 bond lengths are longer and C3−C5 and C8−C10 shorter. For $S1^\alpha$ structures, the C7−C12 bond length is about 1.478 Å independently of the model, a value slightly larger than a typical C−C single bond. The C12−C14 bond lengths take values close to 1.42 Å. In $S1^\beta$ the opposite trend is observed; C12−C14 bond lengths are larger than C7−C12 values.

Table 1 displays the relative energies of the different minima. The stability order depends on the oxo or thio nature of the compound. On the contrary, the acid or ester (thioacid or thioester) nature of the compounds has no effect on the stabilities. For the pCE^- and pCA^- models, the $S1^\beta$ geometry is 0.30 eV more stable than $S1^p$ and 0.25 eV more stable than $S1^\alpha$. In turn, the $S1^\alpha$ minima of models containing sulfur are slightly more stable than $S1^\beta$ structures (about 0.06 eV for $pCTE^-$ and 0.09 eV for $pCTA^-$) and than $S1^p$ (0.13 and 0.15 eV for $pCTE^-$ and $pCTA^-$, respectively).

In a previous study about the absorption spectra of these compounds,[72,88−90] it was found that in the gas phase the most probable transition for all the studied derivatives was that leading to the S1 state, with oscillator strength of about 1.0 in all cases. This transition had a ($\pi \rightarrow \pi^*$) character. The emission process from $S1^P$ goes in the opposite direction, involving the de-excitation from the same orbital and with an oscillator strength close to 1 as well. On the contrary, the oscillator strengths for the transitions between the ground state and $S1^\alpha$ and $S1^\beta$ are practically zero. Hence, emission from these minima is unlikely, and, in principle, only emission from $S1^p$ minima is expected. The energy gap between the $S1^p$ minimum and the ground state (Table 2) is about 2.70 eV for pCE^-/pCA^- and 2.50 eV for $pCTE^-$/$pCTA^-$. Once again, the behavior of oxo and thio compounds is different. On the other hand, the substitution of a hydrogen atom for a bulkier group like methyl, i.e., the change from acid to ester, does not affect the energy values. Turning to the twisted minima, the S1−S0 energy gaps for $S1^\beta$ are much smaller than for $S1^\alpha$. This fact, previously highlighted by Gromov et al.,[18−20] points to the presence of a CI close to $S1^\beta$.

From the above considerations two types of CIs should be, at least, expected: a CI related to the torsion around the single bond, and a CI tied with the double-bond twist. They have been denoted as CI^α and CI^β, respectively. Those MECI optimization calculations starting from planar $S1^p$ structures led to CI^β geometries for the pCE^-/pCA^- pair, whereas CI^α structures were obtained in the case of thio derivatives. In

DOI: 10.1021/acs.jctc.6b01069
J. Chem. Theory Comput. 2017, 13, 737−748

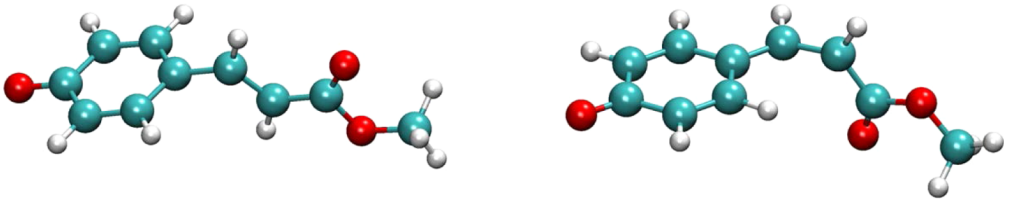

Figure 4. $S1^{\alpha}$ and $S1^{\beta}$ structures for the pCE^{-} model. Similar structures were obtained for pCA^{-}, $pCTE^{-}$, and $pCTA^{-}$.

Table 1. Relative Energies (in eV) for the Different Stationary Points Located on the Gas Phase Excited State Surface of the Four Models at the SA2-CASSCF(12,11)-PT2/cc-pVDZ Level

	pCE^{-}	$pCTE^{-}$	pCA^{-}	$pCTA^{-}$
$S1^{p}$	0	0	0	0
$S1^{\alpha}$	−0.05	−0.13	−0.06	−0.15
$S1^{\beta}$	−0.30	−0.07	−0.30	−0.06

Table 2. S1−S0 Transition Energies (in eV) for the Different Stationary Points Located on the Gas Phase Excited State Surface of the Four Models at the SA2-CASSCF(12,11)-PT2/cc-pVDZ Level[a]

	pCE^{-}	$pCTE^{-}$	pCA^{-}	$pCTA^{-}$
$S1^{p}$	2.69 (0.9)	2.50 (0.9)	2.71 (0.9)	2.51 (0.9)
$S1^{\alpha}$	1.70 (0.0)	1.34 (0.0)	1.69 (0.0)	1.30 (0.0)
$S1^{\beta}$	0.38 (0.0)	0.75 (0.0)	0.40 (0.0)	0.81 (0.0)

[a]Oscillator strength in parentheses.

order to reach CI^{β} structures for the $pCTE^{-}$/$pCTA^{-}$ pair it was necessary to start from strongly twisted configurations around the C12−C14 bond. This fact is probably due to the presence of a substantial barrier related to the β-torsion for those derivatives with a sulfur atom in the carboxylic end. For oxo compounds, it was not possible to obtain CI^{α} structures.

Another interesting point to note is that the CI^{α} structures in thio derivatives (see Table S3 of the Supporting Information) show values for the α angle of about 92° and around 104−105° for the β-torsion, i.e., a concerted mechanism is followed in the path connecting $S1^{p}$ and CI^{α}. As for the CI^{β} structures, α and β torsion present values of around 162° and 73°, respectively. Note that also in this case there is a concerted rotation of both angles, with the peculiarity that now the rotation of α helps the rotation of β, and it is not necessary to arrive to 90° to reach the CI.

As mentioned before, the dynamic correlation contribution to the energy was added *a posteriori* using the CASSCF optimized geometries. The same procedure was followed in the location of the MECIs. Even though this protocol is usually useful, it can happen that the new S0−S1 gap does not fulfill now the CIs existence conditions. Table 3 displays S0−S1 CASSCF and CASPT2 energy gaps for CI geometries calculated at the SA2-CASSCF(12,11)/cc-pVDZ level of theory. Whereas CI^{α} structures for $pCTA^{-}$ and $pCTE^{-}$ models show a very small CASPT2 energy gap and, consequently, these structures correspond also to CIs, this is not the case for CI^{β} geometries. According to the energetic criteria, CI^{β} structures optimized at the SA2-CASSCF level are no longer CIs at the CASPT2 level. In a previous paper[72] it was shown that for pCE^{-} SA2-CASSCF(12,11) and CASPT2(12,11) CI^{β} geometries were very similar. Furthermore, the energy of the excited state hardly depended on the calculation level

Table 3. CASSCF and CASPT2 S1−S0 Energy Differences (eV) for SA2-CASSCF(12,11)/cc-pVDZ CI^{α} and CI^{β} Optimized Structures

	CI^{α}		CI^{β}	
	CASPT2	CASSCF	CASPT2	CASSCF
pCE^{-}			0.42	0.01
$pCTE^{-}$	0.01	0.03	0.71	0.01
pCA^{-}			0.04	0.02
$pCTA^{-}$	0.09	0.01	0.68	0.05

(CASSCF or CASPT2) used during the optimization, and then we could assume that these excited states were well described using CASSCF geometries. The main effect of the dynamic correlation was to stabilize the ground state energy at the MECI geometry, whereas the energy of the excited state was very similar in both CASSCF and CASPT2 geometries.

Figure 5 displays relative stabilities for all the structures located on the S1 surface, including the FC point. Absorption and fluorescence emission are marked with solid and dashed arrows, respectively. This figure can be considered as a summary of the results obtained in the gas phase. For the sake of simplicity, just CASPT2 energies were shown (the dynamic correlation is known to decrease the transition energy values). The energy diagrams show that substitution of a hydrogen atom by a methyl group in the ester part of the molecule does not affect the topology of the excited state, the energy profiles being very similar for pCE^{-}/pCA^{-} and $pCTE^{-}$/$pCTA^{-}$ pairs. However, the stability order of $S1^{p}$, $S1^{\alpha}$, and $S1^{\beta}$ strongly depends on the nature of the heteroatom (oxygen or sulfur) of the ester group. In this way, the $S1^{\beta}$ geometry is the most stable structure for the pCE^{-}/pCA^{-} pair, whereas in thio compounds it is the $S1^{\alpha}$ structure. As for the nonradiative de-excitation paths, our results show that while in oxo compounds only the double bond rotation de-excitation path is possible, in thio compounds both single and double bond rotation paths exist. It is worth noting that, in the gas phase, the CI^{α} and CI^{β} structures present higher energy values than the $S1^{p}$ minima and FC points, and, consequently, they are not accessible from vertical excitation to S1. It follows that for those molecules that do not suffer autoionization, fluorescence would be the preferred de-excitation path.

Table 4 displays the charge distribution for all the critical points of the four molecular models considered. For the sake of simplicity, the systems have been divided in three parts: the phenolic group, the vinyl double bond, and the ester or thioester part. The chromophore ground state features a large negative charge on the phenolic group, being somewhat larger in oxo compounds than in thio compounds; during the vertical absorption, part of this charge is transferred toward the rest of the molecule. At the planar $S1^{p}$ structure, most of the charge is located on the vinyl double bond, being also larger on oxo than in thio compounds. This trend increases in $S1^{\alpha}$, where the

DOI: 10.1021/acs.jctc.6b01069
J. Chem. Theory Comput. 2017, 13, 737−748

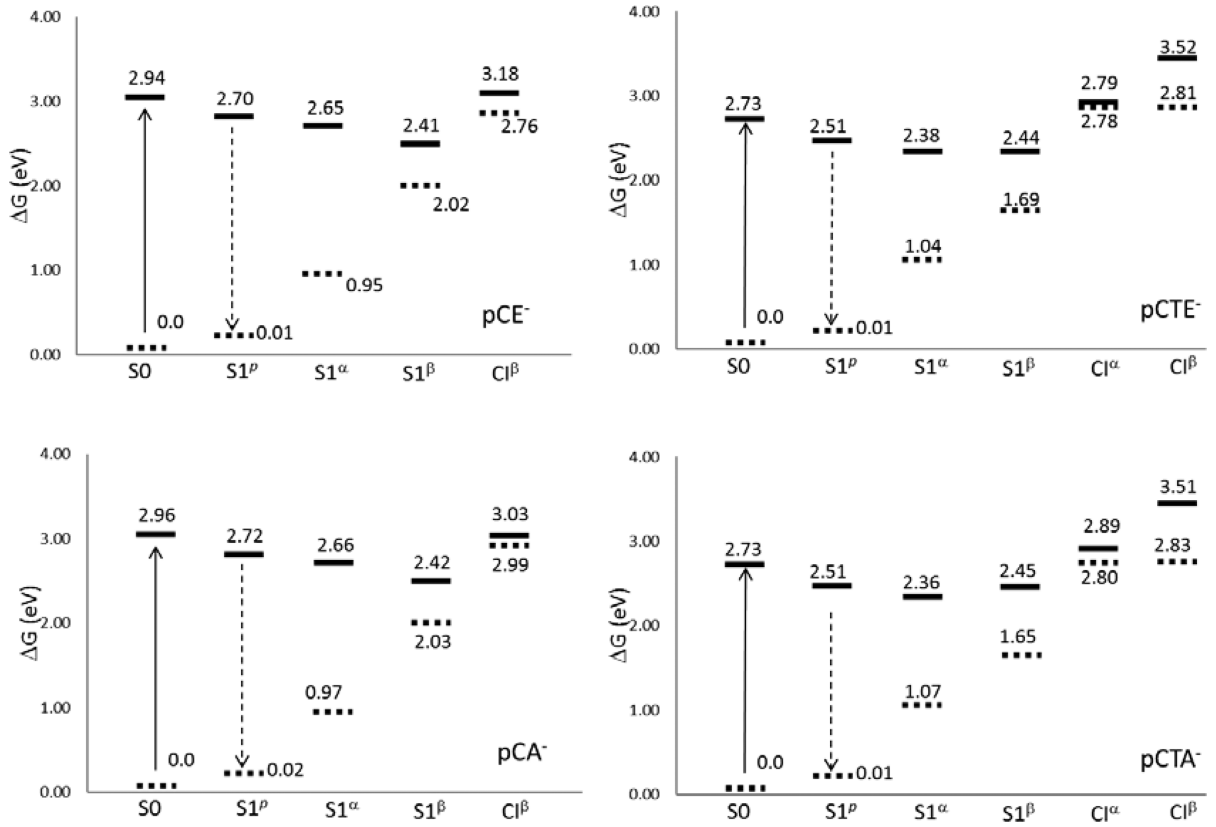

Figure 5. Relative energies with respect to the ground state minimum calculated at the CASPT2//CASSCF/cc-pVDZ level of theory in the gas phase.

Table 4. Gas Phase Charge Distribution for the Ground State and the Different Structures Located on S1[a]

	pCE⁻	pCTE⁻	pCA⁻	pCTA⁻
S0				
phenolic group	−0.626	−0.595	−0.615	−0.589
vinylic double bond	−0.358	−0.287	−0.308	−0.209
CX-Y fragment	−0.016	−0.118	−0.077	−0.202
$S1^p$				
phenolic group	−0.392	−0.426	−0.394	−0.451
vinylic double bond	−0.474	−0.333	−0.414	−0.264
CX-Y fragment	−0.135	−0.241	−0.192	−0.285
$S1^\alpha$				
phenolic group	−0.065	−0.003	0.009	−0.018
vinylic double bond	−0.717	−0.624	−0.726	−0.543
CX-Y fragment	−0.218	−0.373	−0.283	−0.439
$S1^\beta$				
phenolic group	−0.671	−0.657	−0.637	−0.638
vinylic double bond	−0.254	−0.212	−0.247	−0.175
CX-Y fragment	−0.075	−0.131	−0.116	−0.187
CI^α				
phenolic group		−0.006		0.019
vinylic double bond		−0.597		−0.565
CX-Y fragment		−0.397		−0.453
CI^β				
phenolic group	−0.515	−0.550	−0.451	−0.607
vinylic double bond	−0.441	−0.265	−0.452	−0.160
CX-Y fragment	−0.043	−0.185	−0.097	−0.232

[a]For the sake of simplicity the chromophore has been split in three parts, corresponding to the phenolic group, the vinylic double bond and the terminal fragment.

double bond carries a charge that varies between −0.54 and −0.72 *e*. The largest differences between oxo and thio compounds appear in CI^β: in thio compounds most charge is located on the phenolic group, while in oxo compounds the charge is distributed between the phenolic group and the vinylic double bond.

b. Excited State Free Energy Surface in Aqueous Solution. It is well-known that polar solvents can modify the stability and topology of excited states. The four molecules considered in the present study provide examples of this fact; thus, in aqueous solution, the network of hydrogen bonds stabilizes the negative charge of the chromophore and prevents the autoionization of its first excited state that now becomes stable. Furthermore, in this section we show that, contrary to what was found in the gas phase, in water solution 1) the S1 excited state displays only one minimum, the planar structure $S1^p$, the $S1^\alpha$ and $S1^\beta$ structures are no longer minima. 2) CI^α structures are also found for oxo compounds. 3) The relative stability of minima and CIs is reverted with respect to the gas phase values: MECI structures become more stable than the $S1^p$ minimum. As a consequence, three competitive de-excitation channels coexist: fluorescence from $S1^p$, photoisomerization through CI^β, and nonradiative, nonreactive, deexcitation through CI^α. These deactivation channels are similar to those found in pCK⁻, a molecule that has also been used as a model for the PYP chromophore and whose dynamics has been described in detail by Boggio-Pasqua et al.[12] and Martínez and co-workers.[17]

$S1^p$ geometries, see Table S4 in the Supporting Information, are very similar in the gas phase and in solution. It is only worth mentioning the slight increase of the O1−C2, C16−O17, and

DOI: 10.1021/acs.jctc.6b01069
J. Chem. Theory Comput. 2017, 13, 737−748

X18-Y19 bond lengths or the decrease of C16-X18. The solvent also causes small variations in the charge distributions (Table 5). In general a minimal increase in the charge of the phenolic

Table 5. In Solution Charge Distribution for the Ground State and the Different Structures Located on S1

	pCE$^-$	pCTE$^-$	pCA$^-$	pCTA$^-$
S0				
phenolic group	−0.839	−0.921	−0.883	−0.956
vinylic double bond	−0.275	−0.127	−0.128	0.072
CX-Y fragment	0.114	0.048	0.011	−0.016
$S1^p$				
phenolic group	−0.382	−0.507	−0.409	−0.516
vinylic double bond	−0.539	−0.220	−0.428	−0.083
CX-Y fragment	−0.079	−0.272	−0.164	−0.401
CI^α				
phenolic group	−0.024	0.119	−0.003	−0.093
vinylic double bond	−0.921	−0.787	−0.779	−0.469
CX-Y fragment	−0.055	−0.332	−0.219	−0.438
CI^β				
phenolic group	−0.935	−0.792	−0.735	−0.827
vinylic double bond	−0.089	−0.126	−0.169	0.005
CX-Y fragment	0.024	−0.082	−0.096	−0.177

ring is registered, more evident for the pCTE$^-$/pCTA$^-$ pair which loses charge from the central part of the molecule. For the pCE$^-$/pCA$^-$ pair the behavior is somewhat different as the flux of the charge goes from the carboxylic fragment toward the vinyl bond and phenolic ring.

What is more important is the change in the solvent structure around the chromophore when the FC point relaxes until the $S1^p$ minimum. It is worth reminding that when the ground state excites and the system reaches the FC point, the solvent remains in equilibrium with the ground state electron charge distribution. Then, the solute internal degrees of freedom (nuclear and electronic) and the solvent structure relax until they become mutually equilibrated. The new equilibrium differs notably from that existing in the ground state as can be seen comparing the radial distribution functions (*rdf*) for the two states, see Figure 6. Whereas in the ground state the height of the first peak is large in the Ow-O1 *rdf*, very low in the Ow-O17 *rdf* and negligible in the Ow-X18 *rdf*,[90] in the excited state the situation turned into a greater height for the Ow-O17 and the Ow-X18 *rdfs* and a less structured solvent around the phenolic oxygen, although the height of the first peak around O1 is still larger than around O17 and X18. In sum, as a consequence of the flux of charge accompanying the excitation and subsequent relaxation from FC to $S1^p$, the phenolic oxygen atom becomes worse solvated in the excited state than in the ground state, while the opposite is found for the heteroatoms of the ester or thioester group. Radial distribution functions of pCA$^-$ and pCTA$^-$ are similar to those corresponding to pCE$^-$ and pCTE$^-$, respectively, and they are displayed in Figure S1 in the Supporting Information.

Once the solvent structure around the $S1^p$ is known it becomes possible to determine the fluorescence emission. Vertical transition energies and the corresponding solvent shifts are shown in Table 6. The trend is similar to that found in the gas phase. The substitution of the acid hydrogen by a methyl group does not modify the spectrum. This fact reveals the minor role played by this part of the molecule in the emission process (a similar conclusion was obtained in a previous study

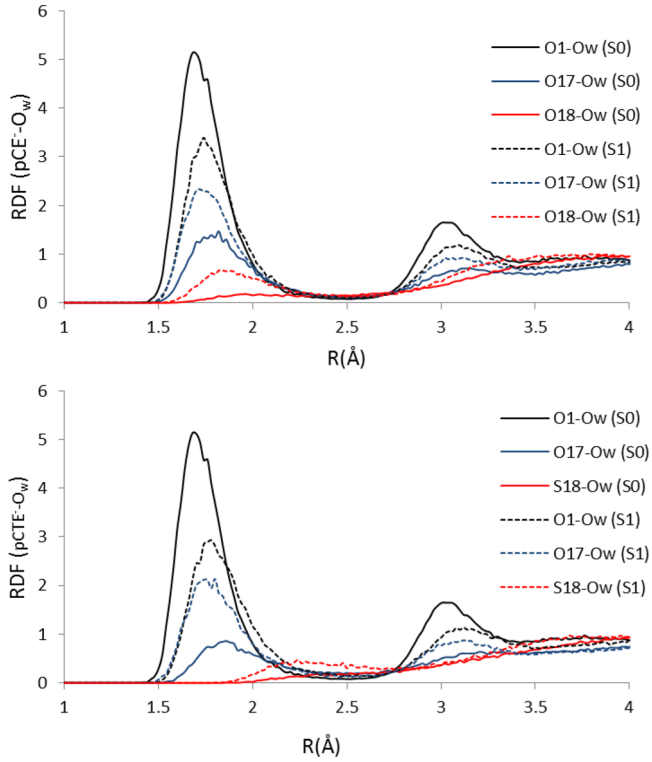

Figure 6. Radial distribution functions for the pCE$^-$ and pCTE$^-$ derivatives in water solution. Ground state in full line and excited state in dotted line.

Table 6. IIn Solution S1−S0 Transition Energies (eV) and Solvent Shifts (eV) for $S1^p$ Structures at SA2-CASSCF(12,11)-PT2/cc-pVDZ Level[a]

	pCE$^-$	pCTE$^-$	pCA$^-$	pCTA$^-$
$S1^p$	2.74 (1.01)	2.51 (1.16)	2.71 (1.00)	2.51 (1.17)
δ ($S1^p$-S0)	0.05	0.01	0.00	0.00

[a]Oscillator strength for each transition in parentheses.

of the absorption spectra[90]). On the contrary, the replacement of the oxygen atom by a sulfur atom shifts the spectrum in some 0.2 eV toward the red. In this way, for the pCE$^-$/pCA$^-$ pair the emission appears at around 2.70 eV, whereas this value is around 2.50 eV for the pCTE$^-$/pCTA pair. These results are in good agreement with those reported by Espagne et al. for pCE$^-$ (2.76 eV[91]) and the pCT$^-$ (phenyl thioester derivative) (2.47 eV[94]). The red shift observed in thio compounds relative to oxo compounds is related to differences in the electron fluxes during the fluorescence: the lower the flux of charge, the lower the energy gap between the excited and ground state. From Table S5 in the Supporting Information, it follows that, as expected, when the system returns to the ground state, the negative charge on the phenolic ring increases. For the pCTE$^-$/pCTA$^-$ pair the flux is lower than for the pCE$^-$/pCA$^-$ pair (≈ −0.1 e vs ≈ −0.2 e, respectively), and, consequently, it displays lower transition energies. The calculated red shift exerted by the sulfur atom agrees with the experimental trend found by Espagne et al.[91,93] The study of different derivatives (pCA^{2-}, pCE$^-$, amide, ketone, and phenyl thioester) reveals a progressive red shift in both the absorption and emission spectra that correlates with the electron acceptor strength of the carbonyl tail.

DOI: 10.1021/acs.jctc.6b01069
J. Chem. Theory Comput. 2017, 13, 737−748

From Table 6, it can be inferred that the solvent effect on the fluorescence spectrum is negligible, and this although the solute−solvent interaction energies are close to 5.64 eV. This differs from the results found in the absorption spectrum, which displays solvent shifts of about 0.8−0.9 eV. The low solvent shift in the emission spectrum is a consequence of the small modification of the chromophore charge distribution during the emission and, what it is more important, of the characteristics of the solvent structure around the chromophore. In S1, solvent molecules concentrate around both moieties (phenolate and ester) of the molecule. During the emission part of the charge is transferred from the ester moiety to the phenolate moiety, and the decrease of the interaction energy of the ester moiety is compensated with the increase in the interaction energy of the phenolate group. This is in contrast with the absorption results. In S0, solvent molecules concentrate around the phenolic oxygen, and the concentration around the ester moiety is negligible. Consequently, when during the excitation the charge moves from the phenolate moiety to the ester moiety, there is a decrease of the interaction energy in the phenolate that is not compensated by an increase of the interaction energy of the ester moiety. Therefore, the large Stokes shift of almost 1 eV found in this system is mainly a consequence of the differences in the solvent structure around the S0 and S1 states. Experiments have confirmed that the position of the fluorescence band hardly depends on the solvent.[93] Additionally, steady-state techniques have revealed that PYP chromophore models are weakly fluorescent, regardless of the nature of the carbonyl group[11,91] in aqueous solution the fluorescence quantum yields have been estimated to be on the order of 0.1%. These facts point to the existence of alternative de-excitation channels that compete with the radiative path. Inside the protein the most probable de-excitation mechanism is the isomerization process leading to the formation of the *cis* isomer, which involves the flipping of the chromophore thioester tail, while the phenolate group of the chromophore remains unaffected.[15,40,95] The situation seems to be different in solution. Thus, experimental studies with different PYP chromophore models reveal that the excited-state relaxation mechanism depends on the oxo or thio character of the molecular model. For instance, Espagne et al.[91,94] found that the PYP chromophore in water, modeled by pCT^-, does not produce any stable *cis* isomer under irradiation, but, after excitation, it relaxes back to the initial *trans* configuration via a short-lived intermediate. The excited state of $pCTE^-$ in water solution returns also the initial *trans* configuration via a short-lived intermediate.[23,55,56,92,94] The behavior of thio derivatives of the PYP chromophore in solution contrasts with the relaxation mechanism reported for models containing an oxygen atom in the ester group. For these derivatives transient spectroscopy studies in water solution have attributed the excited state deactivation to the rotation of the ethylenic bond.[27,28] In fact, the UV−visible absorption spectrum of pCE^-, in basic solution of methanol under steady-state irradiation, displays an isosbestic point that has been attributed to the partial formation of the *cis* isomer.[28]

The different behavior shown by oxo and thio compounds is related to differences in the free energy profile of the S1 state, mainly in the relative stabilities of minima and CIs. As it has been previously indicated, and unlike gas phase results where no CI^{α} structures were found for the oxo compounds, in solution CIs for both α and β torsional angles are found for all the models considered. The interaction with solvent induces changes on the geometries and charge distribution of the CIs. Now CI^{α} and CI^{β} become almost purely α-twisted and β-twisted structures, respectively, i.e., α and β angles of CI in solution agree with the angles displayed by $S1^{\alpha}$ and $S1^{\beta}$ minima in the gas phase. CI^{α} and CI^{β} become now the structures with the lowest energy on S1.

Table 7 displays free-energy differences between all the structures located on the S1 surface for all the models, and

Table 7. Relative Free Energies (in eV) in Water Solution and Their Components at the SA2-CASSCF(12,11)-PT2/cc-pVDZ Level of Theory

		ΔE	ΔG^{int}	ΔG
pCE^-	$S1^p$	0	0	0
	CI^{α}	0.50	−0.81	−0.31
	CI^{β}	−0.03	−1.34	−1.37
$pCTE^-$	$S1^p$	0	0	0
	CI^{α}	−0.11	−0.71	−0.83
	CI^{β}	0.32	−0.99	−0.67
pCA^-	$S1^p$	0	0	0
	CI^{α}	0.39	−0.82	−0.43
	CI^{β}	−0.006	−0.87	−0.88
$pCTA^-$	$S1^p$	0	0	0
	CI^{α}	0.02	−0.06	−0.04
	CI^{β}	0.61	−0.46	0.15

Figure 7 shows the energetic diagram. The results point to the existence of two different nonradiative de-excitation pathways in solution competing with the radiative de-excitation through fluorescence emission. From an energetic point of view, our theoretical results show that, for oxo compounds, CI^{β} structures are more stable than CI^{α}, 1.06 eV for pCE^- and 0.45 eV for pCA^-. The opposite trend is found in thio derivatives where CI^{α} structures are more stable than CI^{β} ones (0.16 eV for $pCTE^-$ and 0.19 eV for $pCTA^-$). Furthermore, contrary to what happens in the gas phase, the CI energies are clearly below the FC and $S1^p$ minima (except for CI^{β} in $pCTA^-$).

It is worth noting that the replacement of the hydrogen atom of the carboxylic group by a methyl group has an important effect on the relative stability of CIs. Thus, the presence of a methyl group increases the relative stability of CI^{β} both in oxo and thio compounds by about 0.40−0.80 eV. As for the stability of CI^{α}, the effect of the methyl group varies depending on the oxo or thio nature of the compound. Thus, it increases its stability in thio compounds, but it decreases it in oxo compounds.

The stability of the different conformers in solution, Table 7, is the result of the interplay between two components (see eq 2): the internal energy component (Δ_E) and the solvation energy (ΔG^{int}). Both in oxo and thio compounds the solvation energies (ΔG^{int}) are higher for CI^{β} structures than for CI^{α} and $S1^p$. The internal energy favors CI^{β} in oxo compounds but CI^{α} in thio compounds. Finally, ΔG^{int} values are higher for oxo compounds and for thio compounds. All these facts taken together provide an explanation of the changes induced by the solvent on the differential stability of the different structures. Thus, in the gas phase the most stable structures on S1 were the $S1^{\alpha}$ and $S1^{\beta}$ minima, the MECIs being higher in energy than the minima and even than the FC point. When the system is solvated, the ground state is more stabilized than the excited state, and this shifts the position of the MECIs, whose geometries overlap now with the $S1^{\alpha}$ and $S1^{\beta}$ gas phase

DOI: 10.1021/acs.jctc.6b01069
J. Chem. Theory Comput. 2017, 13, 737−748

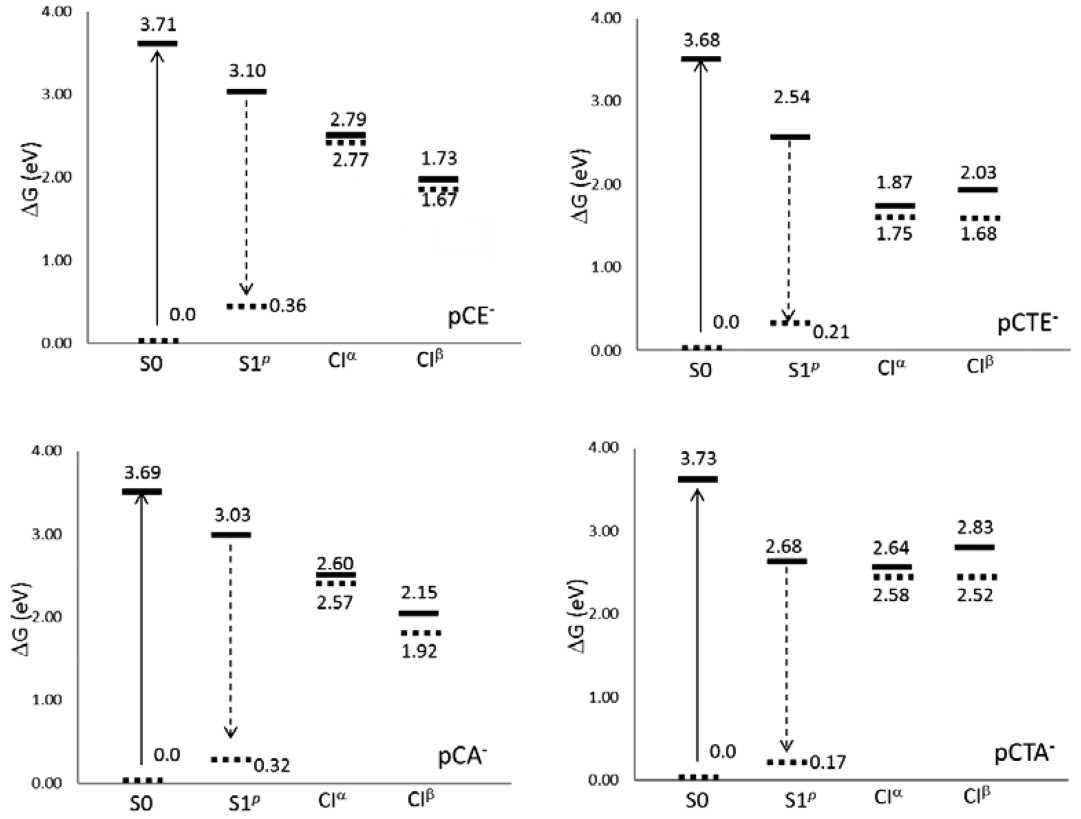

Figure 7. Relative energies with respect to the in equilibrium ground state at the CASPT2//CASSCF/cc-pVDZ level of theory in water solution.

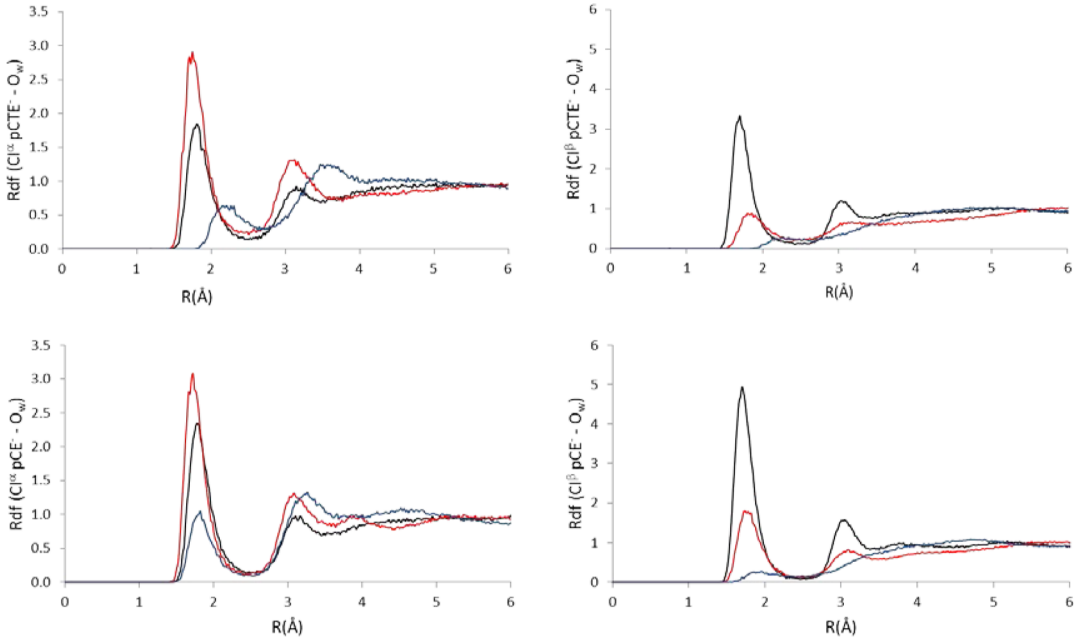

Figure 8. Radial distribution functions for the CI^{α} and CI^{β} structures of pCE^{-} and $pCTE^{-}$ derivatives in water solution. Black line for O1-Ow, red line for O17-Ow and blue line for X18-Ow rdf pairs.

geometries. CIs become now the most stable structures (on the S1 surface) in water solution. The $S1^{p}$ minimum is the only one that remains in solution; however, it is found at larger energies than the MECIs, and, consequently, a low fluorescence quantum yield is expected. Our results provide a theoretical basis to the experimental observations where the *trans*—*cis* isomerization is the preferred deactivation route for models containing an oxygen atom, while models with a sulfur atom follow an alternative route with no formation of the *cis* isomer.

Finally, Figure 8 shows the rdfs for CI^{α} and CI^{β} structures. Obviously, given that we are assuming equilibrium solvation they are related with the solute charge distribution. The CI^{β} charge distribution is very similar to that displayed by S0—in the two structures the charge is localized on the phenolic

DOI: 10.1021/acs.jctc.6b01069
J. Chem. Theory Comput. 2017, 13, 737−748

oxygen—and accordingly they display very similar rdfs. There are very well-defined peaks around O1 and O17, the rdf height being larger in oxo compounds than in thio compounds as the O1 atom carries a larger charge in the former. Consequently, CI^{β} is more stabilized in oxo compounds. On the contrary the height of the peak around O17 is larger for CI^{α} than for CI^{β} and in oxo than in thio compounds. O17 carries a very small charge in oxo compounds but large in thio compounds. Hence, the stability of CI^{α} is larger in thio than in oxo compounds.

In sum, when the molecule relaxes from FC to S1 some water molecules move from the phenyl group to the vinyl bond. CI^{α} concentrates most of the charge in the vinyl group, and it is around this region where the density of water molecules is larger. Additionally, the solvent structure around the phenolic group disappears and increases around the carbonyl group. Finally, the solvent structure around CI^{β} is similar to that found around S0. These facts suggest that very important solvent reorganization is necessary before the molecule reaches the CI.

V. CONCLUSIONS

Many biological processes (vision, phototaxis, proton-pumping, etc.) have as a first step a photoisomerization reaction. Because of its small size and structural simplicity, the *p*-coumaric acid is a good system where to study solvent effects or the influence of the acid/ester and oxo/thio nature of the chromophore on de-excitation channels. Our calculations show that, in agreement with the experimental evidence, oxo and thio derivatives follow different de-excitation paths. Additionally, it can be concluded that the presence of a bulkier group in the carbonyl tail does not affect the relative stability order, but it can modify the free energy differences and, consequently, it modulates the competition between de-excitation channels.

In the gas phase the only de-excitation route seems to be emission from a planar minimum, $S1^{p}$. This process, however, is hardly observed as the S1 state is above the autoionization threshold. When the system is dissolved in water, there is a dramatic change in the free energy surface of the first excited state. The first effect is that now the first excited states are stable with respect to autoionization. This opens the possibility of de-excitation through fluorescence emission, photoisomerization of the central double bond, or a nonradiative channel through CI^{α}. Except in $pCTA^{-}$ where the CI^{β} channel is probably closed as its energy is above the $S1^{p}$ minimum, in the remaining compounds the three channels could be open. However, from the analysis of the free energy differences it becomes evident that the photoisomerization seems to be the preferred route in oxo compounds, while in thio compounds the nonradiative, nonreactive, de-excitation route through CI^{α} is favored. These results agree with the experiments and evidence that the analysis of the free energy surfaces, despite its static nature, can shed light on the competition between de-excitation channels.

■ ASSOCIATED CONTENT

Supporting Information

The Supporting Information is available free of charge on the ACS Publications website at DOI: 10.1021/acs.jctc.6b01069.

Selected geometrical parameters for the different minima and conical intersections in the gas phase and in water solution for the four chromophore models (pCE^{-}, $pCTE^{-}$, pCA^{-}, $pCTA^{-}$), optimized geometries at the SA2-CASSCF(12,11)/cc-pVDZ level of theory, in solution charge distribution for $S1^{p}$ and the ground state at $S1^{p}$ geometry (S0*) (PDF)

■ AUTHOR INFORMATION

Corresponding Author

*E-mail: memartin@unex.es.

ORCID

M. Elena Martín: 0000-0002-5252-2893

Notes

The authors declare no competing financial interest.

■ ACKNOWLEDGMENTS

This work was supported by the GR15169 project from the Consejería de Economía, Comercio e Innovación of the Gobierno de Extremadura.

■ REFERENCES

(1) Meyer, T. E. *Biochim. Biophys. Acta, Bioenerg.* **1985**, *806*, 175.
(2) Meyer, T. E.; Yakali, E.; Cusanovich, M. A.; Tollin, G. *Biochemistry* **1987**, *26*, 418.
(3) Baca, M.; Borgstahl, G. E. O.; Boissinot, M.; Burke, P. M.; Williams, D. R.; Slater, K. A.; Getzoff, E. D. *Biochemistry* **1994**, *33*, 14369.
(4) Hoff, W. D.; Düx, P.; Hård, K.; Devreese, B.; Nugteren-Roodzant, I. M.; Crielaard, W.; Boelens, R.; Kaptein, R.; van Beeumen, J.; Hellingwerf, K. J. *Biochemistry* **1994**, *33*, 13959.
(5) Baltuška, A.; van Stokkum, I. H. M.; Kroon, A.; Monshouwer, R.; Hellingwerf, K. J.; van Grondelle, R. *Chem. Phys. Lett.* **1997**, *270*, 263.
(6) Chosrowjan, H.; Mataga, N.; Nakashima, N.; Imamoto, Y.; Tokunaga, R. *Chem. Phys. Lett.* **1997**, *270*, 267.
(7) Devanathan, S.; Pacheco, A.; Ujj, L.; Cusanovich, M. A.; Tollin, G.; Lin, S.; Woodbury, N. *Biophys. J.* **1999**, *77*, 1017.
(8) Sprenger, W. W.; Hoff, W. D.; Armitage, J. P.; Hellingwerf, K. J. *J. Bacteriol.* **1993**, *175*, 3096.
(9) Hellingwerf, K. J.; Hendriks, J.; Gensch, T. *J. Phys. Chem. A* **2003**, *107*, 1082.
(10) Cusanovich, M. A.; Meyer, T. E. *Biochemistry* **2003**, *42*, 4759.
(11) Changenet-Barret, P.; Espagne, A.; Plaza, P.; Hellingwerf, K. J.; Martin, M. M. *New J. Chem.* **2005**, *29*, 527.
(12) Boggio-Pasqua, M.; Burmeister, C. F.; Robb, M. A.; Groenhof, G. *Phys. Chem. Chem. Phys.* **2012**, *14*, 7912.
(13) Kort, R.; Vonk, H.; Xu, X.; Hoff, W. D.; Crielaard, W.; Hellingwerf, K. J. *FEBS Lett.* **1996**, *382*, 73.
(14) Getzoff, E. D.; Gutwin, K. N.; Genick, U. K. *Nat. Struct. Biol.* **2003**, *10*, 663.
(15) Heyne, K.; Mohammed, O. F.; Usman, A.; Dreyer, J.; Nibbering, E. T. J.; Cusanovich, M. A. *J. Am. Chem. Soc.* **2005**, *127*, 18100.
(16) Boggio-Pasqua, M.; Robb, M. A.; Groenhof, G. *J. Am. Chem. Soc.* **2009**, *131*, 13580.
(17) Ko, C.; Virshup, A. M.; Martínez, T. J. *Chem. Phys. Lett.* **2008**, *460*, 272.
(18) Gromov, E. V. *J. Chem. Phys.* **2014**, *141*, 224308.
(19) Gromov, E. V.; Burghardt, I.; Hynes, J. T.; Köppel, H.; Cederbaum, L. S. *J. Photochem. Photobiol., A* **2007**, *190*, 241.
(20) Gromov, E. V.; Burghardt, I.; Köppel, H.; Cederbaum, L. S. *J. Phys. Chem. A* **2011**, *115*, 9237.
(21) Kukura, P.; McCamant, E. W.; Yoon, S.; Wandschneider, D. B.; Mathies, R. A. *Science* **2005**, *310*, 1006.
(22) Wang, Q.; Schoenlein, R. W.; Peteanu, L. A.; Mathies, R. A.; Shank, C. A. *Science* **1994**, *266*, 422.
(23) Larsen, D. S.; Vengris, M.; van Stokkum, I. H. M.; van der Horst, M. A.; de Weerd, F. L.; Hellingwerf, K. J.; van Grondelle, R. *Biophys. J.* **2004**, *86*, 2538.
(24) Lammich, L.; Rajput, J.; Andersen, L. H. *Phys. Rev. E* **2008**, *78*, 51916.

DOI: 10.1021/acs.jctc.6b01069
J. Chem. Theory Comput. 2017, 13, 737−748

(25) Zhu, J.; Paparelli, L.; Hospes, M.; Arents, J.; Kennis, J. T. M.; van Stokkum, I. H. M.; Hellingwerf, K. J.; Groot, M. L. *J. Phys. Chem. B* **2013**, *117*, 11042.
(26) Mooney, C. R. S.; Parkes, M. A.; Iskra, A.; Fielding, H. H. *Angew. Chem., Int. Ed.* **2015**, *54*, 5646.
(27) Espagne, A.; Changenet-Barret, P.; Plaza, P.; Martin, M. M. *J. Phys. Chem. A* **2006**, *110*, 3393.
(28) Espagne, A.; Paik, D. H.; Changenet-Barret, P.; Plaza, P.; Martin, M. M.; Zewail, A. H. *Photochem. Photobiol. Sci.* **2007**, *6*, 780−787.
(29) Groenhof, G.; Bouxin-Cademartory, M.; Hess, B.; de Visser, S. P.; Berendsen, H. J. C.; Olivucci, M.; Mark, A. E.; Robb, M. A. *J. Am. Chem. Soc.* **2004**, *126*, 4228.
(30) Groenhof, G.; Schäfer, L. V.; Boggio-Pasqua, M.; Grubmüller, H.; Robb, M. A. *J. Am. Chem. Soc.* **2008**, *130*, 3250.
(31) Lee, I.-R.; Lee, W.; Zewail, A. H. *Proc. Natl. Acad. Sci. U. S. A.* **2006**, *103*, 258.
(32) Nakamura, R.; Hamada, N.; Abe, K.; Yoshizawa, M. *J. Phys. Chem. B* **2012**, *116*, 14768.
(33) Philip, A. F.; Nome, R. A.; Papadantonakis, G. A.; Scherer, N. F.; Hoff, W. D. *Proc. Natl. Acad. Sci. U. S. A.* **2010**, *107*, 5821.
(34) Devanathan, S.; Lin, S.; Cusanovich, M. A.; Woodbury, N.; Tollin, G. *Biophys. J.* **2000**, *79*, 2132.
(35) Chosrowjan, H.; Mataga, N.; Shibata, Y.; Imamoto, Y.; Tokunaga, F. *J. Phys. Chem. B* **1998**, *102*, 7695.
(36) Gromov, E. V.; Burghardt, I.; Köppel, H.; Cederbaum, L. S. *J. Photochem. Photobiol., A* **2012**, *234*, 123.
(37) Gromov, E. V.; Burghardt, I.; Köppel, H.; Cederbaum, L. S. *J. Phys. Chem. A* **2011**, *115*, 9237.
(38) Stahl, A. D.; Hospes, M.; Singhal, K.; van Stokkum, I.; van Grondelle, R.; Groot, M. L.; Hellingwerf, K. J. *Biophys. J.* **2011**, *101*, 1184.
(39) Groot, M. L.; van Wilderen, L. J. G. W.; Larsen, D. S.; van der Horst, M. A.; van Stokkum, I. H. M.; Hellingwerf, K. J.; van Grondelle, R. *Biochemistry* **2003**, *42*, 10054.
(40) Sigala, P. A.; Tsuchida, M. A.; Herschlag, D. *Proc. Natl. Acad. Sci. U. S. A.* **2009**, *106*, 9232.
(41) Rocha-Rinza, T.; Christiansen, O.; Rajput, J.; Gopalan, A.; Rahbek, D. B.; Andersen, L. H.; Bochenkova, A. V.; Granovsky, A. A.; Bravaya, K. B.; Nemukhin, A. V.; Christiansen, K. L.; Nielsen, M. B. *J. Phys. Chem. A* **2009**, *113*, 9442.
(42) Putschögl, M.; Zirak, P.; Penzkofer, A. *Chem. Phys.* **2008**, *343*, 107.
(43) Gromov, E. V.; Burghardt, I.; Köppel, H.; Cederbaum, L. S. *J. Am. Chem. Soc.* **2007**, *129*, 6798.
(44) He, Z.; Martin, C. H.; Birge, R.; Freed, K. F. *J. Phys. Chem. A* **2000**, *104*, 2939.
(45) Yamada, A.; Yamamoto, S.; Yamato, T.; Kakitani, T. *J. Mol. Struct.: THEOCHEM* **2001**, *536*, 195.
(46) Brudler, R.; Meyer, T. E.; Genick, U. K.; Devanathan, S.; Woo, T. T.; Millar, D. P.; Gerwert, K.; Cusanovich, M. A.; Tollin, G.; Getzoff, E. D. *Biochemistry* **2000**, *39*, 13478.
(47) Isborn, C. M.; Götz, A. W.; Clark, M. A.; Walker, R. C.; Martínez, T. J. *J. Chem. Theory Comput.* **2012**, *8*, 5092.
(48) Virshup, A. M.; Punwong, C.; Pogorelov, T. V.; Lindquist, B. A.; Ko, C.; Martínez, T. J. *J. Phys. Chem. B* **2009**, *113*, 3280.
(49) Wang, Y.; Li, H. *J. Chem. Phys.* **2010**, *133*, 034108.
(50) Toniolo, A.; Granucci, G.; Martínez, T. J. *J. Phys. Chem. A* **2003**, *107*, 3822.
(51) Okamoto, K.; Hamada, N.; Okamura, T.-A.; Ueyama, N.; Yamamoto, H. *Org. Biomol. Chem.* **2009**, *7*, 3782.
(52) Mohammed, O. F.; Heyne, K.; Usman, A.; Dreyer, J.; Nibbering, E. T. J.; Cusanovich, M. A. In *Ultrafast Phenomena XV*; Corkum, P., Jonas, D., Miller, R. J. D., Weiner, A. M., Eds.; Springer Series in Chemical Physics, Springer: Berlin, Germany, 2007; Vol. *88*, p 453.
(53) Ma, Y.; Rohlfing, M.; Molteni, C. *J. Chem. Theory Comput.* **2010**, *6*, 257.
(54) Coto, P. B.; Roca-Sanjuán, D.; Serrano-Andrés, L.; Martín-Pendás, A.; Martí, S.; Andrés, J. *J. Chem. Theory Comput.* **2009**, *5*, 3032.
(55) Larsen, D. S.; Vengris, M.; van Stokkum, I. H. M.; van der Horst, M. A.; Cordfunke, R. A.; Hellingwerf, K. J.; van Grondelle, R. *Chem. Phys. Lett.* **2003**, *369*, 563.
(56) Vengris, M.; van der Horst, M. A.; Zgrablic, G.; van Stokkum, I. H. M.; Haacke, S.; Chergui, M.; Hellingwerf, K. J.; van Grondelle, R.; Larsen, D. S. *Biophys. J.* **2004**, *87*, 1848.
(57) Sánchez, M. L.; Aguilar, M. A.; Olivares del Valle, F. J. *J. Comput. Chem.* **1997**, *18*, 313.
(58) Fdez. Galván, I.; Sánchez, M. L.; Martín, M. E.; Olivares del Valle, F. J.; Aguilar, M. A. *Comput. Phys. Commun.* **2003**, *155*, 244.
(59) Martín, M. E.; Sánchez, M. L.; Aguilar, M. A.; Olivares del Valle, F. J. *J. Mol. Struct.: THEOCHEM* **2001**, *537*, 213.
(60) Almeida, G. G.; Cordeiro, J. M. M.; Martín, M. E.; Aguilar, M. A. *J. Chem. Theory Comput.* **2016**, *12*, 1514.
(61) Sánchez, M. L.; Martín, M. E.; Fdez. Galván, I.; Olivares del Valle, F. J.; Aguilar, M. A. *J. Phys. Chem. B* **2002**, *106*, 4813.
(62) Fdez. Galván, I.; Sánchez, M. L.; Martín, M. E.; Olivares del Valle, F. J.; Aguilar, M. A. *J. Chem. Phys.* **2003**, *118*, 255.
(63) Okuyama-Yoshida, N.; Nagaoka, M.; Yamabe, T. *Int. J. Quantum Chem.* **1998**, *70*, 95.
(64) Okuyama-Yoshida, N.; Kataoka, K.; Nagaoka, M.; Yamabe, T. *J. Chem. Phys.* **2000**, *113*, 3519.
(65) Hirao, H.; Nagae, Y.; Nagaoka, M. *Chem. Phys. Lett.* **2001**, *348*, 350.
(66) Sánchez, M. L.; Martín, M. E.; Fdez. Galván, I.; Olivares del Valle, F. J.; Aguilar, M. A. *J. Phys. Chem. B* **2002**, *106*, 4813.
(67) Levine, B. G.; Coe, J. D.; Martínez, T. J. *J. Phys. Chem. B* **2008**, *112*, 405.
(68) Muñoz-Losa, A.; Martín, M. E.; Fdez. Galván, I.; Aguilar, M. A. *Chem. Phys. Lett.* **2007**, *443*, 76.
(69) Muñoz-Losa, A.; Fdez. Galván, I.; Sánchez, M. L.; Martín, M. E.; Aguilar, M. A. *J. Phys. Chem. B* **2008**, *112*, 877.
(70) Muñoz-Losa, A.; Martín, M. E.; Fdez. Galván, I.; Aguilar, M. A. *J. Chem. Theory Comput.* **2011**, *7*, 4050.
(71) Zwanzig, R. W. *J. Chem. Phys.* **1954**, *22*, 1420.
(72) García-Prieto, F. F.; Muñoz-Losa, A.; Martín, M. E.; Aguilar, M. A. *Phys. Chem. Chem. Phys.* **2016**, *18*, 27476.
(73) Aquilante, F.; De Vico, L.; Férre, N.; Ghigo, G.; Malmqvist, P.-Å.; Neogrády, P.; Pedersen, T.; Pitoňak, M.; Reiher, M.; Roos, B. O.; Serrano-Andrés, L.; Urban, M.; Veryazov, V.; Lindh, R. *J. Comput. Chem.* **2010**, *31*, 224.
(74) Berendsen, H. J. C.; van der Spoel, D.; van Drunen, R. *Comput. Phys. Commun.* **1995**, *91*, 43.
(75) Lindahl, E.; Hess, B.; van der Spoel, D. *J. Mol. Model.* **2001**, *7*, 306.
(76) Dunning, T. H. *J. Chem. Phys.* **1989**, *90*, 1007.
(77) Andersson, K.; Malmqvist, P.-Å.; Roos, B. O.; Sadlej, A. J.; Wolinski, K. J. *J. Phys. Chem.* **1990**, *94*, 5483.
(78) Andersson, K.; Malmqvist, P.-Å.; Roos, B. O. *J. Chem. Phys.* **1992**, *96*, 1218.
(79) Zobel, J. P.; Nogueira, J. J.; González, L. *Chem. Sci.* **2016**, DOI: 10.1039/C6SC03759C.
(80) Muñoz-Losa, A.; Fdez. Galván, I.; Aguilar, M. A.; Martín, M. E. *J. Chem. Theory Comput.* **2013**, *9*, 1548.
(81) Jorgensen, W. L.; Tirado-Rives, J. *J. Am. Chem. Soc.* **1988**, *110*, 1657.
(82) Jorgensen, W. L.; Maxwell, D. S.; Tirado-Rives, J. *J. Am. Chem. Soc.* **1996**, *118*, 11225.
(83) Daday, C.; Curutchet, C.; Sinicropi, A.; Mennucci, B.; Filippi, C. *J. Chem. Theory Comput.* **2015**, *11*, 4825.
(84) Jorgensen, W. L.; Madura, J. D. *Mol. Phys.* **1985**, *56*, 1381.
(85) Darden, T.; York, D.; Pedersen, L. *J. Chem. Phys.* **1993**, *98*, 10089.
(86) Nosé, S. *Mol. Phys.* **1984**, *52*, 255.
(87) Hoover, W. G. *Phys. Rev. A: At., Mol., Opt. Phys.* **1985**, *31*, 1695.
(88) García-Prieto, F. F.; Fdez. Galván, I.; Muñoz-Losa, A.; Aguilar, M. A.; Martín, M. E. *J. Chem. Theory Comput.* **2013**, *9*, 4481.
(89) Frutos Puerto, S.; Muñoz-Losa, A.; Martín, M. E.; Aguilar, M. A. *Comput. Theor. Chem.* **2014**, *1040-1041*, 287.

DOI: 10.1021/acs.jctc.6b01069
J. Chem. Theory Comput. 2017, 13, 737−748

(90) García-Prieto, F. F.; Aguilar, M. A.; Fdez. Galván, I.; Muñoz-Losa, A.; Olivares del Valle, F. J.; Sánchez, M. L.; Martín, M. E. *J. Phys. Chem. A* **2015**, *119*, 5504.
(91) Espagne, A.; Paik, D. H.; Changenet-Barret, P.; Martin, M. M.; Zewail, A. H. *ChemPhysChem* **2006**, *7*, 1717.
(92) Changenet-Barret, P.; Espagne, A.; Charier, S.; Baudin, J. B.; Jullien, L.; Plaza, P.; Hellingwerf, K. J.; Martin, M. M. *Photochem. Photobiol. Sci.* **2004**, *3*, 823.
(93) Espagne, A.; Changenet-Barret, P.; Baudin, J. B.; Plaza, P.; Martin, M. M. *J. Photochem. Photobiol., A* **2007**, *185*, 245.
(94) Changenet-Barret, P.; Espagne, A.; Katsonis, N.; Charier, S.; Baudin, J. B.; Jullien, L.; Plaza, P.; Martin, M. M. *Chem. Phys. Lett.* **2002**, *365*, 285.
(95) Pande, K.; Hutchison, C. D. M.; Groenhof, G.; Aquila, A.; Robinson, J. S.; Tenboer, J.; Basu, S.; Boutet, S.; DePonte, D. P.; Liang, M.; White, T. A.; Zatsepin, N. A.; Yefanov, O.; Morozov, D.; Oberthuer, D.; Gati, C.; Subramanian, G.; James, D.; Zhao, Y.; Koralek, J.; Brayshaw, J.; Kupitz, C.; Conrad, C.; Roy-Chowdhury, S.; Coe, J. D.; Metz, M.; Xavier, P. L.; Grant, T. D.; Koglin, J. E.; Ketawala, G.; Fromme, R.; Šrajer, V.; Henning, R.; Spence, J. C. H.; Ourmazd, A.; Schwander, P.; Weierstall, U.; Frank, M.; Fromme, P.; Barty, A.; Chapman, H. N.; Moffat, K.; van Thor, J. J.; Schmidt, M. *Science* **2016**, *352*, 725.

DOI: 10.1021/acs.jctc.6b01069
J. Chem. Theory Comput. 2017, 13, 737−748